SCIENCE CHINA
Earth Sciences

• RESEARCH PAPER •

October 2017 Vol.60 No.10: 1838–1853
doi: 10.1007/s11430-016-9061-3

Variations in soil moisture over the 'Huang-Huai-Hai Plain' in China due to temperature change using the CNOP-P method and outputs from CMIP5

SUN GuoDong[1,3*], PENG Fei[1,3,4] & MU Mu[1,2]

[1] *State Key Laboratory of Numerical Modeling for Atmospheric Sciences and Geophysical Fluid Dynamics (LASG), Institute of Atmospheric Physics, Chinese Academy of Sciences, Beijing 100029, China;*
[2] *Institute of Atmospheric Sciences, Fudan University, Shanghai 200433, China;*
[3] *University of Chinese Academy of Sciences, Beijing 100049, China;*
[4] *Numerical Weather Prediction Center, China Meteorological Administration, Beijing 100081, China*

Received October 19, 2016; accepted May 26, 2017; published online July 13, 2017

Abstract In this study, the variations in surface soil liquid water (SSLW) due to future climate change are explored in the 'Huang-Huai-Hai Plain' ('3H') region in China with the Common Land Model (CoLM). To evaluate the possible maximum response of SSLW to climate change, the combination of the conditional nonlinear optimal perturbation related to the parameter (CNOP-P) approach and projections from 10 general circulation models (GCMs) of the Coupled Model Intercomparison Project 5 (CMIP5) are used. The CNOP-P-type temperature change scenario, a new type of temperature change scenario, is determined by using the CNOP-P method and constrained by the temperature change projections from the 10 GCMs under a high-emission scenario (the Representative Concentration Pathway 8.5 scenario). Numerical results have shown that the response of SSLW to the CNOP-P-type temperature scenario is stronger than those to the 11 temperature scenarios derived from the 10 GCMs and from their ensemble average in the entire '3H' region. In the northern region, SSLW under the CNOP-P-type scenario increases to 0.1773 m^3 m^{-3}; however, SSLW in the scenarios from the GCMs fluctuates from 0.1671 to 0.1748 m^3 m^{-3}. In the southern region, SSLW decreases, and its variation (–0.0070 m^3 m^{-3}) due to the CNOP-P-type scenario is higher than each of the variations (–0.0051 to –0.0026 m^3 m^{-3}) due to the scenarios from the GCMs.

Keywords CNOP-P, Surface soil liquid water, CMIP5, Climate change, Seasonal and regional heterogeneity

Citation: Sun G D, Peng F, Mu M. 2017. Variations in soil moisture over the 'Huang-Huai-Hai Plain' in China due to temperature change using the CNOP-P method and outputs from CMIP5. Science China Earth Sciences, 60: 1838–1853, doi: 10.1007/s11430-016-9061-3

1. Introduction

Soil moisture plays an important role in the climate system. For instance, it influences the separation of precipitation into surface runoff and infiltration as well as the partitioning of net radiation into latent heat flux and sensible heat flux. The persistence of soil moisture anomalies could affect floods, droughts (Bonan and Stillwell-Soller, 1998; Wu and Zhang, 2013), extreme hot days (Hirschi et al., 2011), heat waves (Lorenz et al., 2010), etc. In climate models, the reasonable representation of soil moisture has been shown to contribute to improving sub-seasonal and seasonal forecasting (Conil et al., 2006; Koster et al., 2004). For agriculture, soil moisture information is vital for crop yields and irrigation scheduling (Tao et al., 2003).

Due to climate change, components of the terrestrial hydrological cycle have changed, such as runoff and streamflow (Aich et al., 2014; Yang et al., 2011; Wang G Q et al., 2012; Peng et al., 2017). The impacts of climate change on hydrological characteristics are typically evaluated using climate

* Corresponding author (email: sungd@mail.iap.ac.cn)

change scenarios, which are generally determined by the climatic outputs from general circulation models (GCMs), as the climatic inputs in a hydrological model. For constructing climate change scenarios, two approaches are commonly used. One is to use hypothetical scenarios (Dan et al., 2012; Mehrotra, 1999) in which a constant (percent) change is added to an observed baseline. Dan et al. (2012) have applied this approach to project the hydrological changes in the Huang-Huai-Hai Plain (3H) region of China. Another method is to apply the downscaled outputs from GCMs to account for the change in climate variability, in which the changes in climatology and climate variability are both considered (Chen et al., 2012; Sperna Weiland et al., 2012). A characteristic of the method is to supply a possible and comprehensive climate change scenario. However, due to the uncertainties in climate modeling (Dobler et al., 2012), downscaling methods (Chen et al., 2013), and hydrological modeling (Bastola et al., 2011), great uncertainty exists in modeling the hydrological responses to climate change.

Another characteristic of using the outputs from GCMs is to present the seasonal and regional heterogeneity in climate change. In China, warming is more significant in winter and spring (Chen and Frauenfeld, 2014a; Ding et al., 2006; Ren et al., 2012). For precipitation, its increase in summer is higher over part of eastern China (Chen and Frauenfeld, 2014a). Additionally, the changes in summer rainfall over China primarily exhibited a decadal change in spatial distribution in recent decades (Zhang et al., 2013; Zhang, 2015). Based on a multi-model ensemble of 20 GCMs from Phase 5 of the Coupled Model Intercomparison Project (CMIP5), the increases in temperature are projected to be greater over northern China and the Tibetan Plateau by the end of the twenty-first century (Chen and Frauenfeld, 2014b). Therefore, it is necessary to introduce seasonal and regional change information on climate change when the hydrological impacts of climate change are evaluated. Although there are some merits in using the outputs of GCMs to discuss the uncertainty of the hydrological changes due to the changing climate, the uncertainty of the hydrological changes may be underestimated for the limited climate change scenarios from the limited GCMs.

To explore the maximum possible variation of the hydrological changes using the climate change scenarios from GCMs, the approach of conditional nonlinear optimal perturbation related to model parameters (CNOP-P) is employed, which is proposed by Mu et al. (2010) and is an optimization method. The CNOP-P represents a type of model parameter and could determine the upper uncertainty bound of the numerical simulation and forecast error. The CNOP-P approach has been applied in studying ENSO predictability (Duan and Zhang, 2010), the transition to the Kuroshio large meander (KLM) state (Wang Q et al., 2012), variations in terrestrial ecosystems (Sun and Mu, 2011, 2012, 2013, 2014, 2017b), and identifications of sensitive and important parameter combinations in numerical models (Sun and Mu, 2017a). There are many studies on how to obtain CNOP-P (Chen et al., 2015), which lead to the comprehensive application of CNOP-P.

By considering the uncertainty of future climate change in different seasons and regions, the combination of the CNOP-P approach and outputs from GCMs may provide a type of climate change scenario to disclose the maximum possible response of the hydrological cycle to future possible climate changes in the study area. The type of climate change scenario determined by the above-mentioned combination could be applied to investigate the maximum uncertainty of numerical simulations and additionally display the seasonal and regional characteristics of climate change within the range projected by GCMs. In this study, temperature is only considered to be a forcing parameter in the hydrological model. The CNOP-P approach and 10 GCMs with high spatial resolutions from CMIP5 along with the Common Land Model (CoLM; Dai et al., 2003) are used to obtain a CNOP-P-type temperature change scenario to comprehensively evaluate the hydrological changes caused by future temperature change alone. The CNOP-P-type temperature change scenario represents a scenario type that could cause the maximum variation of simulated hydrological variables under a reasonable temperature range projected by many GCMs.

Furthermore, the monthly temperature change series (i.e., the difference between the projected monthly temperature and the historical monthly temperature) projected by each GCM, which also show the seasonal and regional temperature change features, are deemed as a type of future temperature change scenario as well and applied to investigate the possible responses of the hydrological cycle to various temperature change scenarios. As a component of the hydrological cycle, soil moisture plays an important role in the climate system, which has been indicated above. In addition, numerous studies of the surface soil liquid water (i.e., soil liquid water in the top 10 cm soil layer; SSLW for short) have been used and analyzed (e.g., Dan et al., 2012; Liu et al., 2014). Consequently, we primarily focus on the responses of SSLW to climate change in this study.

2. Study region, model, and methods

2.1 The study region

The study region is located in eastern China, corresponding to the area from 30°N to 40°N and from 110°E to 120°E. In this study region, the Huang-Huai-Hai Plain (3H) region, one of the nine principal agricultural zones in China, is included where soil moisture has been demonstrated to play an important role in affecting agricultural production (Dan et al., 2012) and climate variability (Zhang and Zuo, 2011; Zuo and

Zhang, 2007). For convenience, the study region is referred to as the 'Huang-Huai-Hai Plain' ('3H') region, which is different from the 3H region. According to the study of Ma and Fu (2005), the semi-humid and semi-arid zones are primarily located in the '3H' region.

2.2 The CoLM model

In this paper, the CoLM model is employed to investigate the impacts of regional and seasonal temperature change on SSLW. It has been tested through extensive offline simulations using a variety of observational data, which have demonstrated that the CoLM model could simulate different land surface processes reasonably (Liu and Lin, 2005; Song et al., 2009; Xin et al., 2006). The model was also employed to explore the parameter sensitivity (Wang et al., 2013). Furthermore, it has been coupled with the National Center for Atmospheric Research (NCAR) Community Climate Model (CCM3) (Zeng et al., 2002). This coupled run has indicated that the CoLM model improves the simulations of surface air temperature, runoff, and snow mass significantly compared to the original NCAR land surface model (LSM).

To run the CoLM model, the Princeton forcing dataset (Sheffield et al., 2006) is used. It is a high-resolution (1.0°×1.0°, 3-hourly), global, meteorological forcing dataset and has been applied to simulate soil moisture in China (Li and Ma, 2010; Wang et al., 2011). Because the CoLM model prefers to use the time step at 30 minutes, the Princeton forcing dataset within our study region has been interpolated into 30-minute intervals with the temporal interpolation programs provided by the developers of the CoLM model. For precipitation, the interpolation program is a statistical approach provided by the Second Global Soil Wetness Project (GSWP2). For other variables, the interpolations are all based on the Cubic Spline method, apart from the downward shortwave radiation interpolation, in which the sun elevation is considered. Then the interpolated dataset is applied to drive the CoLM model for conducting control simulations as the reference states.

Moreover, there are 10 unevenly spaced soil layers in the CoLM model. The thicknesses of the first three layers are 1.75, 2.76 and 4.55 cm in order (9.06 cm in total). Thus, SSLW is approximately calculated as the weighted average of the soil liquid water (SLW) in the first three soil layers according to the soil layer thicknesses. Specifically, the formula to determine the SSLW is as follows:

$$SSLW = \left(1.75 \times SLW_{\text{first soil layer}} + 2.76 \times SLW_{\text{second soil layer}} + 4.55 \times SLW_{\text{third soil layer}}\right) / 9.06 .$$

For the surface soil layer, the net water input is primarily associated with precipitation, soil ice, evapotranspiration (*ET*), and surface runoff (*R*sur). Consequently, SSLW is closely related to precipitation, soil ice, ET and *R*sur.

The soil moisture data from ERA-Interim and the Global Soil Moisture Data Bank has been used to evaluate the CoLM model in simulating SSLW over the '3H' region. The CoLM model could capture the spatial distribution and seasonal variations of SSLW (see Appendix Figures S1 and S2 (available at http://earth.scichina.com)). As a result, it is feasible to apply the CoLM model in exploring the responses of SSLW to climate change.

2.3 The conditional nonlinear optimal perturbation related to parameter (CNOP-P)

For the readers' convenience, an introduction to the CNOP-P approach is presented. Assume the nonlinear differential equations as follows:

$$\begin{cases} \dfrac{\partial \boldsymbol{U}}{\partial t} = F(\boldsymbol{U}, \boldsymbol{P}) \ \ \boldsymbol{U} \in R^n, t \in [0, T], \\ \boldsymbol{U}\big|_{t=0} = \boldsymbol{U}_0, \end{cases} \tag{1}$$

where F is a nonlinear operator; $\boldsymbol{U}_0$ represents an initial value of the state variable $\boldsymbol{U}$; and $\boldsymbol{P}$ stands for a parameter vector. Let M_t be the propagator of eq. (1) from the initial time 0 to t. Then, the solution $\boldsymbol{U}(t)$ at time t could be written as $M_t(\boldsymbol{U}_0, \boldsymbol{P})$. Suppose that there is a perturbation to the parameter vector $\boldsymbol{P}$, denoted as $\boldsymbol{p}$. Then, the solution of eq. (1) changes into M_t ($\boldsymbol{U}_0$, $\boldsymbol{P}$+$\boldsymbol{p}$) and is denoted by $\boldsymbol{U}(t)$+$\boldsymbol{u}(t)$. Here, $\boldsymbol{u}(t)$ describes the departure from the reference state $\boldsymbol{U}(t)$, which is induced by the parameter perturbation vector $\boldsymbol{p}$.

For a specified time T and norm, the parameter perturbation $\boldsymbol{p}_\delta$ is called a CNOP-P with the constraint condition $\boldsymbol{p} \in \Omega$, if and only if,

$$J(\boldsymbol{p}_\delta) = \max_{\boldsymbol{p} \in \Omega} J(\boldsymbol{p}), \tag{2}$$

where

$$J(\boldsymbol{p}) = \|\boldsymbol{u}(T)\| = \left\|M_T(\boldsymbol{U}_0, \boldsymbol{P}+\boldsymbol{p}) - M_T(\boldsymbol{U}_0, \boldsymbol{P})\right\| . \tag{3}$$

$\boldsymbol{P}$ is the reference state of parameters and generally represents the standard parameter values in a numerical model. $\boldsymbol{p}$ is the perturbation to the parameter reference state and represents parameter errors. CNOP-P represents a type of parameter perturbation that satisfies certain constraints and causes the maximum departure of the studied state variable from its reference state, at time T.

In this paper, $\boldsymbol{P}$ is the forcing parameter associated with temperature and $\boldsymbol{p}$ could be regarded as the change in temperature, and the L2 norm is chosen. For our study, CNOP-P is regarded as a type of temperature perturbation that could consider the regional and seasonal changes in temperature, and it causes the maximum variations in soil moisture.

2.4 Experimental design

In previous studies, only perturbations to the annual temperature are discussed (Sun and Mu, 2012, 2014), as shown in

eqs. (4) and (5).

$$\frac{\sum_{y=1}^{N}\sum_{m=1}^{12}\sum_{i=1}^{d(y,m)}\sum_{n=1}^{r}(P_{t,y,m,i,n}+p_{t,y})}{r\times\sum_{y=1}^{N}\sum_{m=1}^{12}d(y,m)} = \frac{\sum_{y=1}^{N}\sum_{m=1}^{12}\sum_{i=1}^{d(y,m)}\sum_{n=1}^{r}P_{t,y,m,i,n}}{r\times\sum_{y=1}^{N}\sum_{m=1}^{12}d(y,m)}+\delta_t, \quad (4)$$

$$0\le p_{t,y}\le\sigma_t. \quad (5)$$

Here, $P_{t,y,m,i,n}$ is the time-variant forcing parameter associated with temperature and represents the temperature reference state. $p_{t,y}$ represents the perturbation to the temperature reference state and remains unchanged in a year. In addition, δ_t is the change in temperature climatology and is determined by the potential future regional averaged temperature variation, which is invariable in the whole study region.

However, many studies have demonstrated that climate change varies with regions and seasons (Ding et al., 2006; Ren et al., 2012; Zhang et al., 2013; Zhang, 2015). To explore the impacts of regional and seasonal temperature changes on SSLW, a modified experimental design is proposed as follows:

$$\frac{\sum_{y=1}^{N}\sum_{m=1}^{12}\sum_{i=1}^{d(y,m)}\sum_{n=1}^{r}(P_{t,s,y,m,i,n}+p_{t,s,y,m})}{r\times\sum_{y=1}^{N}\sum_{m=1}^{12}d(y,m)} = \frac{\sum_{y=1}^{N}\sum_{m=1}^{12}\sum_{i=1}^{d(i,j)}\sum_{n=1}^{r}P_{t,s,y,m,i,n}}{r\times\sum_{y=1}^{N}\sum_{m=1}^{12}d(y,m)}+\delta_{s,t}, \quad (6)$$

$$\sigma_{t,s,y,m,l}\le p_{t,s,y,m}\le\sigma_{t,s,y,m,u}. \quad (7)$$

Here, s represents each grid in the study region. Subscripts y, m and i represent year, month, and day, respectively; $d(y,m)$ is the number of days in a month. r represents the number of measurements conducted in a day, which depends on the temporal resolution of the forcing dataset. $p_{t,s,y,m}$ is the perturbation to the temperature reference state and stays the same in a month. Moreover, it is hypothesized to be unaltered for all months in a season. In spring, for example, there is the following relationship: $p_{t,s,y,3}=p_{t,s,y,4}=p_{t,s,y,5}$. $p_{t,s,y,m}$ represents the temperature perturbation in each season. In addition, $p_{t,s,y,m}$ is constrained by both $\sigma_{t,s,y,m,l}$ and $\sigma_{t,s,y,m,u}$, which represent the minimum and maximum seasonal temperature perturbations. $\delta_{s,t}$ is the perturbation to the temperature climatology in each grid. As a result, the regional and seasonal dependence of temperature change is considered in the new temperature change scenarios denoted by eqs. (6) and (7).

To determine the parameters $\delta_{s,t}$, $\sigma_{t,s,y,m,l}$ and $\sigma_{t,s,y,m,u}$ in eqs. (6) and (7) to obtain future possible temperature change scenarios, the temperature datasets from 10 GCMs (Table 1) under a high emission scenario RCP8.5 from CMIP5 are analyzed (Taylor et al., 2012). In this emission scenario, RCP8.5 corresponds to the pathway with the highest greenhouse gas emissions. In our study, the impact of climate change due to a high emission scenario RCP8.5 on the soil moisture is evaluated. In detail, the monthly temperature data from each GCM are first bilinear-interpolated to the resolution of 1°×1°, which is in accordance with the forcing dataset. Here, the bilinear interpolation method we use could be expressed as the following formula:

$$\begin{aligned} f(x,y) = {} & \frac{f(x_1,y_1)}{(x_2-x_1)(y_2-y_1)}(x_2-x)(y_2-y) \\ & +\frac{f(x_2,y_1)}{(x_2-x_1)(y_2-y_1)}(x-x_1)(y_2-y) \\ & +\frac{f(x_1,y_2)}{(x_2-x_1)(y_2-y_1)}(x_2-x)(y-y_1) \\ & +\frac{f(x_2,y_2)}{(x_2-x_1)(y_2-y_1)}(x-x_1)(y-y_1). \end{aligned}$$

Then, the projected period of 2011−2100 is divided into 9

Table 1 The list of 10 GCMs from CMIP5[a)]

Model name	Model ID	Country of origin	Resolution (Lat.×Lon.)
ACCESS1-0	M01	Australia	1.875°×1.25°
CCSM4	M02	USA	1.25°×0.9°
CNRM-CM5	M03	France	~1.4°×1.4°
Fgoals-s2	M04	China	~2.81°×1.66°
HadGEM2-AO	M05	Korea	1.875°×1.25°
HadGEM2-CC	M06	United Kingdom	1.875°×1.25°
IPSL-CM5A-MR	M07	France	2.5°×1.25°
MIROC5	M08	Japan	~1.4°×1.4°
MPI-ESM-LR	M09	Germany	1.875°×1.875°
MRI-CGCM3	M10	Japan	1.125°×1.125°

a) Only soil moisture simulations from the GCMs in bold font are employed in our study

slices with the time length of 10 years, which is the same as the length of our study period (1991−2000; N=10). For each model and grid, the difference between the equal-weighted average of the monthly temperature series in all time slices and the historical monthly temperature series from 1991 to 2000, is considered to be a possible monthly temperature change series in the future 10 years and referred to as $T_{s,c,y,m}$ (y=1,...,N; m=1,...,12; and c indicates each model). Thus, the mean value of each future possible monthly temperature change series (i.e., $\sum_{y=1}^{N}\sum_{m=1}^{12} T_{s,c,y,m} / (12 \times N)$) represents the change in temperature climatology. Finally, the variation of temperature climatology ($\delta_{s,t}$) is calculated as the ensemble average of the possible temperature climatology changes based on 10 GCMs (i.e., $\sum_{c=1}^{10}\sum_{y=1}^{N}\sum_{m=1}^{12} T_{s,c,y,m} / (N \times 10 \times 12)$). The minimum and maximum perturbations to the temperature reference state ($\sigma_{t,s,y,m,l}$ and $\sigma_{t,s,y,m,u}$) are the minimum and maximum changes among the monthly temperature changes from all selected GCMs in all months of the season in each year, respectively. For instance, in spring, the upper and lower bounds of the perturbation $p_{t,s,y,m}$ could be characterized by the following formula:

$$\begin{aligned}\sigma_{t,s,y,3(4,5),l} &= \min_{c=1,\,10}\{T_{s,c,y,3},\, T_{s,c,y,4},\, T_{s,c,y,5}\},\\ \sigma_{t,s,y,3(4,5),u} &= \max_{c=1,\,10}\{T_{s,c,y,3},\, T_{s,c,y,4},\, T_{s,c,y,5}\}.\end{aligned} \tag{8}$$

There are many temperature scenarios satisfying the given constraints in eqs. (6) and (7). Among these scenarios, a scenario that induces the maximum changes of SSLW could be obtained by applying the CNOP-P approach, denoted as the CNOP-P-type temperature change scenario. As demonstrated above, the CNOP-P-type temperature change scenario considers the regional and seasonal features of future temperature change.

To compare the impacts of different temperature change scenarios on SSLW, the future possible monthly temperature change series from all GCMs and their ensemble average (hereinafter referred to as the ensemble monthly temperature change series), called 'the GCM-based temperature change scenarios', are also used. These GCM-based scenarios also consider the regional and seasonal temperature change. In addition, the ensemble monthly temperature change series causes the same climatology change as the CNOP-P-type temperature change scenario.

Finally, there are two primary reasons for us to choose the 10 GCMs from CMIP5, which are introduced in Table 1. One is that they have higher spatial resolutions that are close to the spatial resolution of the forcing dataset and helpful for conducting interpolations. Furthermore, the selected GCMs could capture the temperature and precipitation in the '3H' region (see Appendix Figures S3–S8).

3. Results and analysis

In this section, the impacts of different temperature change scenarios on the SSLW are investigated and compared, which comprehensively take the variations of both regional and seasonal temperature into account. For analyzing the hydrological processes that might account for the SSLW changes, the physical processes that influence the variations of the SSLW related to the surface water budget (such as surface soil ice, ET and Rsur) are also explored.

3.1 The impacts of different future temperature change scenarios on SSLW

Figure 1 describes the monthly temperature change series under the CNOP-P-type and GCM-based future temperature change scenarios. The CNOP-P-type temperature change scenario is reasonable and is within the scope defined by the temperature change scenarios from the 10 GCMs. Due to

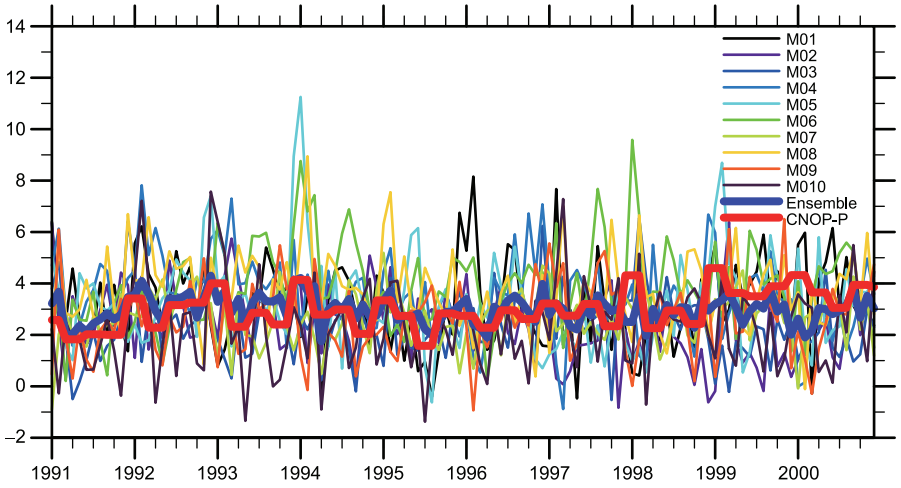

Figure 1 The monthly temperature change series averaged in the '3H' region from 1991 to 2000 due to the CNOP-P-type and GCM-based temperature change scenarios.

these change scenarios, the changes in SSLW are shown in Figure 2. It is shown that the SSLW change due to the CNOP-P-type temperature change scenario is stronger than those due to the 11 temperature change scenarios from the GCMs. In addition, there are different impacts of the temperature scenarios on SSLW in different regions. The primary hydrological processes that contribute to the SSLW changes also vary with the regions. North of 36°N, soil ice melting, indicated by the decrease of surface soil ice (Figure 3), increases SSLW. Both ET and Rsur change slightly (Figures 4 and 5), playing little role in the variations of SSLW. In the south, the changes in soil ice and Rsur are small (Figures 3 and 5). The enhanced ET causes water loss in the soil column (Figure 4) and primarily accounts for the changes of SSLW in this region.

To understand the regional differences due to different temperature change scenarios, the regional averaged SSLW in the north and south is studied. Using 36°N as a boundary, Figure 6 shows the annual SSLW of different sub-regions in the final year of the study period (the year 2000) under the CNOP-P-type and all GCM-based temperature change scenarios. We can see that SSLW under the CNOP-P-type temperature scenario is greatest in the north (Figure 6a) and smallest in the south (Figure 6b). Because of the common SSLW reference state, it is implied that the CNOP-P-type scenario induces the maximum variation extent of SSLW for the final year. Additionally, the maximum SSLW change extent in the north is 0.0099 $m^3\ m^{-3}$ compared to the referenced SSLW (0.1674 $m^3\ m^{-3}$), and −0.0070 $m^3\ m^{-3}$ in the south compared to the referenced SSLW (0.2612 $m^3\ m^{-3}$). For the ensemble temperature change series, SSLW increases by just 0.0039 $m^3\ m^{-3}$ in the north and decreases by 0.0041 $m^3\ m^{-3}$ in the south. Due to other GCM-based temperature change

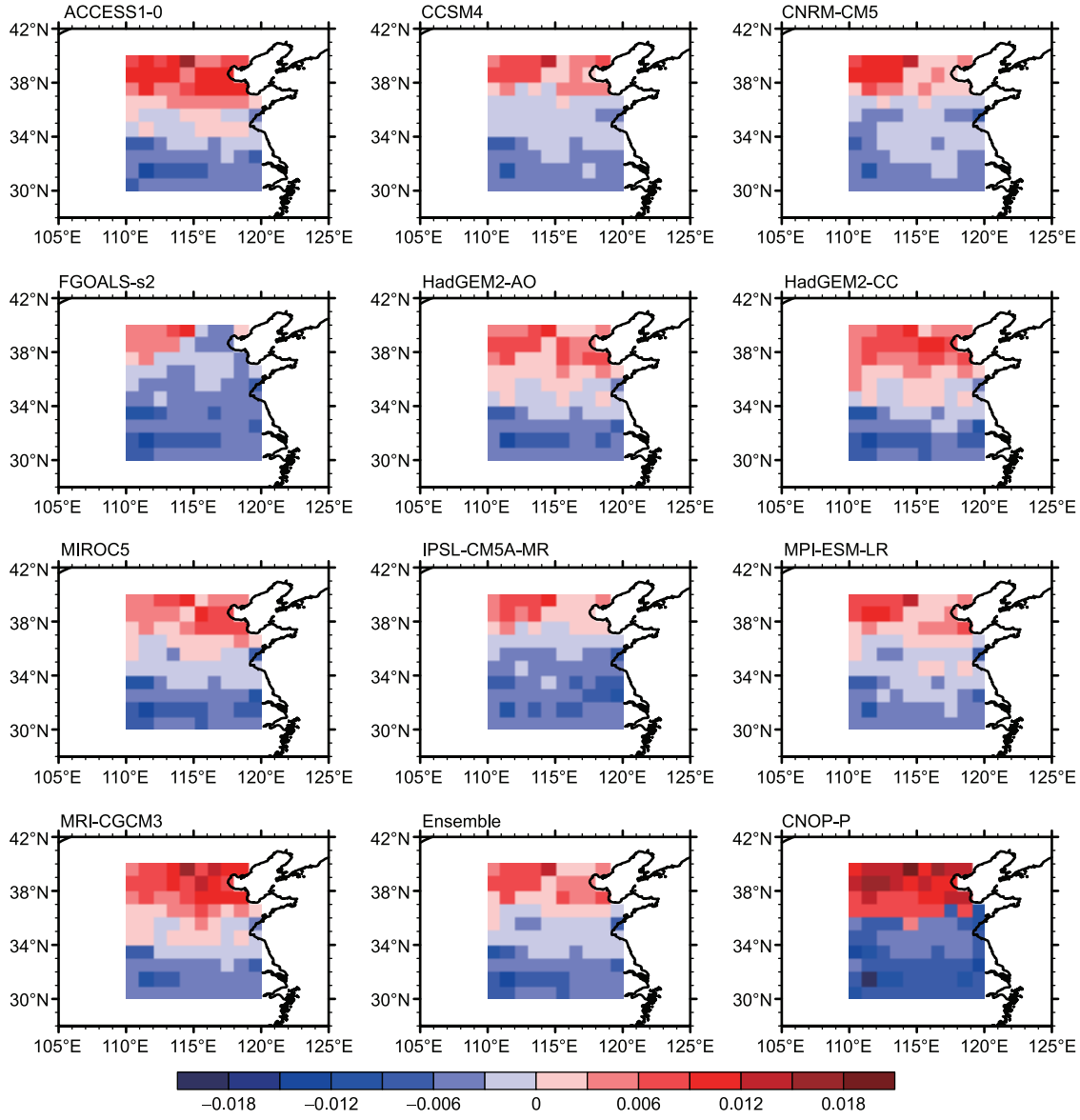

Figure 2 The changes in SSLW ($m^3\ m^{-3}$) due to the CNOP-P-type and GCM-based future possible temperature change scenarios.

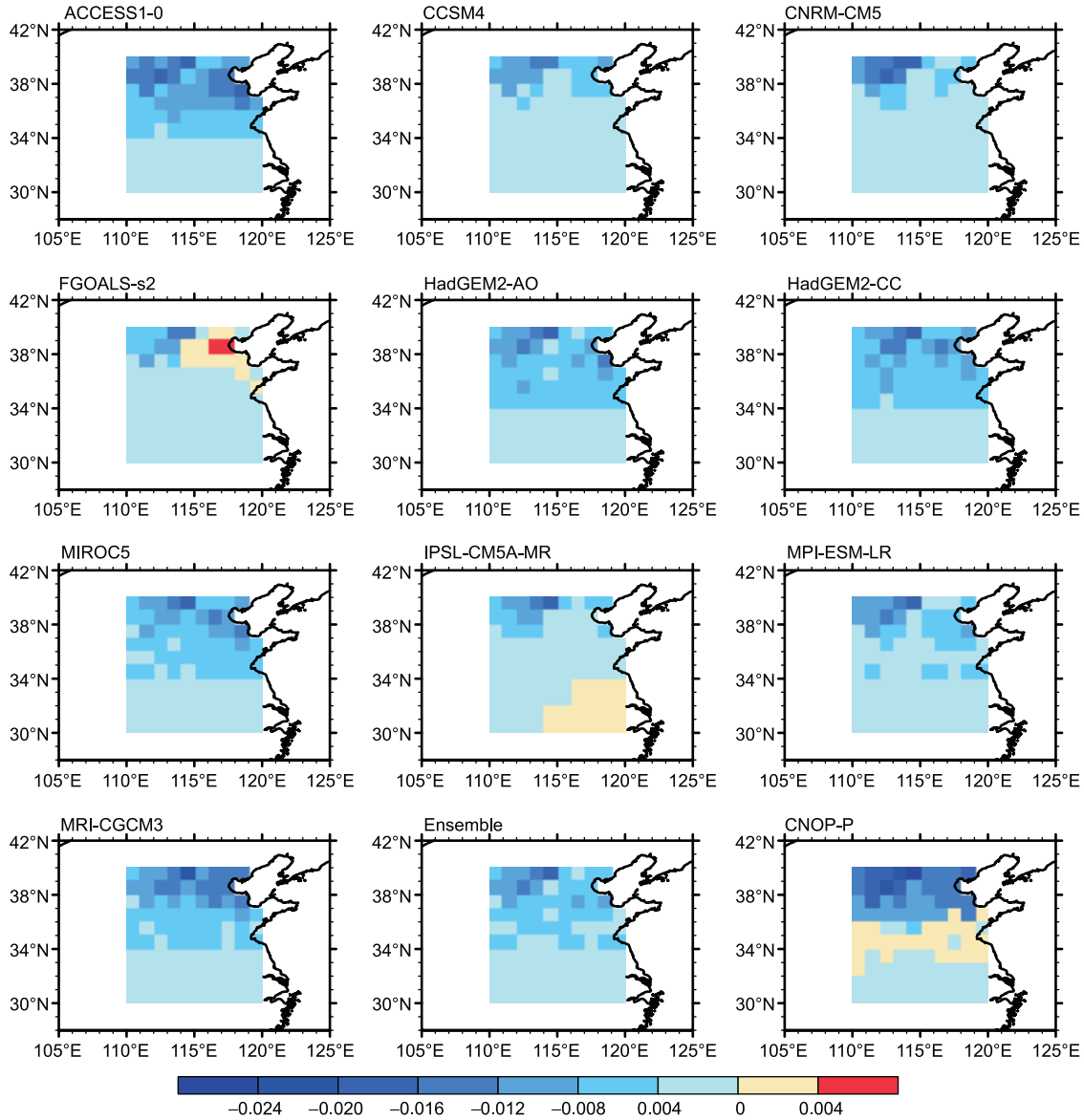

Figure 3 The changes in surface soil ice ($m^3\ m^{-3}$) due to the CNOP-P-type and GCM-based future possible temperature change scenarios.

scenarios, the regional averaged SSLW variations range from 0.0003 to 0.0074 $m^3\ m^{-3}$ in the north and fluctuate from −0.0051 to −0.0026 $m^3\ m^{-3}$ in the south.

There are differences in the hydrological processes that induce the SSLW variations due to different temperature change scenarios. The regional averaged soil ice, *ET* and *R*sur are examined for the final year in the north and south of 36°N across the '3H' region, which are shown in Figures 7–9, respectively. Over the northern region, both *ET* and Rsur change slightly. Due to each temperature change scenario, soil ice melts. For the CNOP-P-type scenario, soil ice is smallest in this region (Figure 7a) and, thus, the melting of soil ice is the most significant (0.0127 $m^3\ m^{-3}$) compared to the referenced soil ice (0.0209 $m^3\ m^{-3}$), contributing to the greatest increase of SSLW. Over the southern region, the changes in soil ice and Rsur are small. The temperature variations increase ET. Compared with other temperature change scenarios, the CNOP-P-type scenario has the maximum ET (Figure 8b). In other words, it leads to the largest ET increase (0.1422 mm day^{-1}) compared to the reference ET (1.8044 mm day^{-1}), thus, resulting in the largest SSLW decrease.

3.2 The variations of seasonal SSLW

Here, the changes of annual SSLW have been presented. In this section, the SSLW change in each season due to the seasonal temperature perturbations will be discussed. Here, only results related to the CNOP-P-type temperature scenario and the ensemble temperature change series are introduced in detail. Because changes in only one year (the year 2000) are calculated, the season 'winter' refers to the months of Jan-

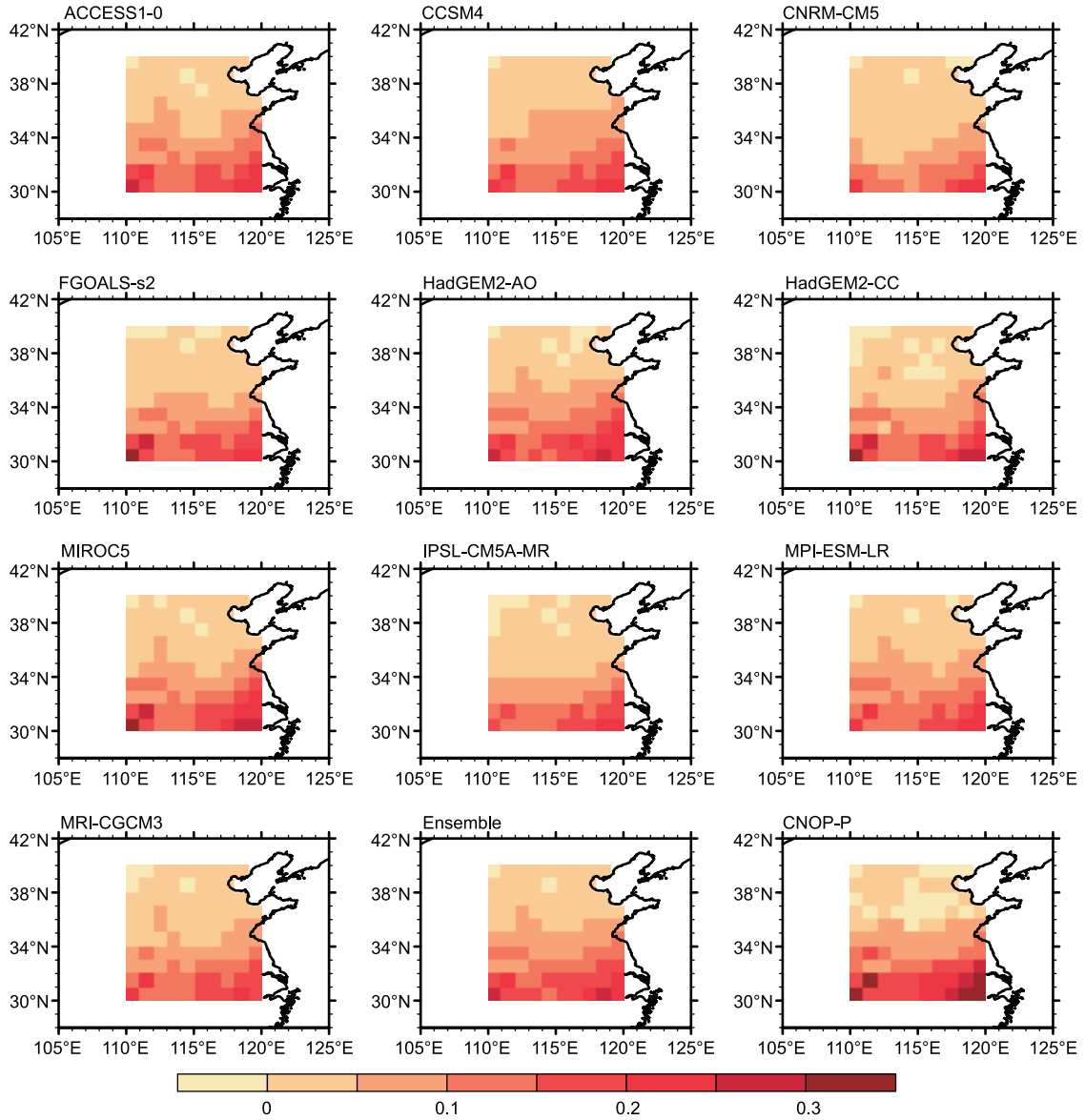

Figure 4 The changes in *ET* (mm day^{-1}) due to the CNOP-P-type and GCM-based future possible temperature change scenarios.

uary, February, and December in the same year in the following section.

In Figure 10, the SSLW changes in all the seasons of the year 2000 are displayed. It shows that the overall SSLW changes in each season induced by the CNOP-P-type scenario are similar to those induced by the ensemble temperature change series. North of 36°N, SSLW is reduced in spring, summer, and autumn (Figure 10); however, it is significantly increased in winter (Figure 10d1 and 10d2). As a result, the increase of SSLW in the winter offsets the decreases of SSLW in the other seasons and contributes to the annual SSLW increase in the northern region. Nevertheless, the SSLW changes in the winter due to the CNOP-P-type scenario are much higher than those due to the ensemble temperature change series. The temperature increases under the CNOP-P-type scenario are larger and lead to more soil ice melting. In addition, the SSLW in the winter averaged over this northern region increases by 0.0399 m^3 m^{-3} due to the CNOP-P-type scenario and by 0.0196 m^3 m^{-3} due to the ensemble temperature change series compared to the referenced SSLW (0.0900 m^3 m^{-3}). In the remaining region, SSLW is reduced in all seasons, especially in the spring (Figure 10a1 and 10a2). In the spring, the average SSLW in the southern region decreases by 0.0083 m^3 m^{-3} due to the CNOP-P-type scenario and by 0.0062 m^3 m^{-3} due to the ensemble temperature change series compared to the referenced SSLW (0.2071 m^3 m^{-3}).

Furthermore, with the boundary 36°N, the area-averaged SSLW in all seasons are shown in Table 2 for all temperature change scenarios. In the north, SSLW is altered slightly in the spring, summer and autumn for all temperature scenarios. In the winter, SSLW is increased under all scenarios. The

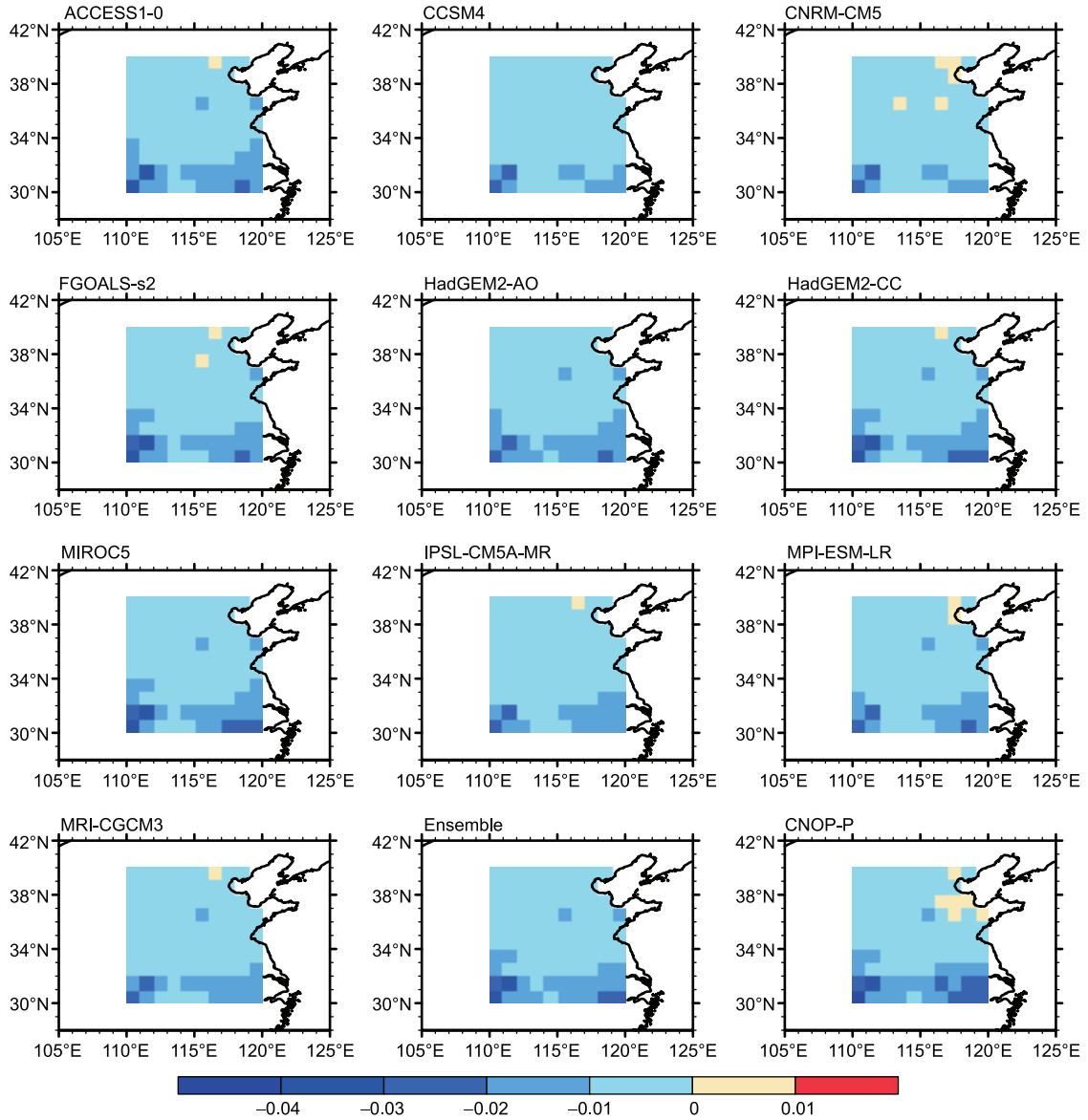

Figure 5 The changes in *R*sur (mm day^{-1}) due to the CNOP-P-type and GCM-based future possible temperature change scenarios.

CNOP-P-type scenario leads to the largest SSLW (i.e., the largest SSLW increase; Table 2), which corresponds to the smallest soil ice volume in this season (i.e., the highest soil ice melting; Table 3) due to the possible temperature changes considered in this study. All the temperature scenarios cause the soil ice to melt in the winter. The melting of soil ice is most significant under the CNOP-P-type scenario (0.0460 m^3 m^{-3}) compared to the referenced soil ice (0.0783 m^3 m^{-3}). However, in the spring, summer, and autumn, changes in soil ice volumes are small. Over the southern region, SSLW diminishes in the spring, summer, autumn, and winter for almost all the temperature scenarios (Table 2), which could be explained by the enhanced ET in almost all of the seasons (Table 4). Generally, under these temperature change scenarios, the SSLW change in the spring is greater. Because Rsur plays an insignificant role in SSLW variations due to temperature change, its seasonal variations are not given here.

4. Discussion

4.1 Why are the variations of precipitation not discussed?

In this study, the impacts of temperature change on soil moisture are investigated. The variation of precipitation is an important factor that directly drives the changes in SSLW. Its amount and frequency both play important roles in the soil moisture dynamics. However, the influences of regional and seasonal changes associated with precipitation on SSLW are not explored. Initially, we tried to introduce the precipitation change by adding the monthly precipitation perturbations to

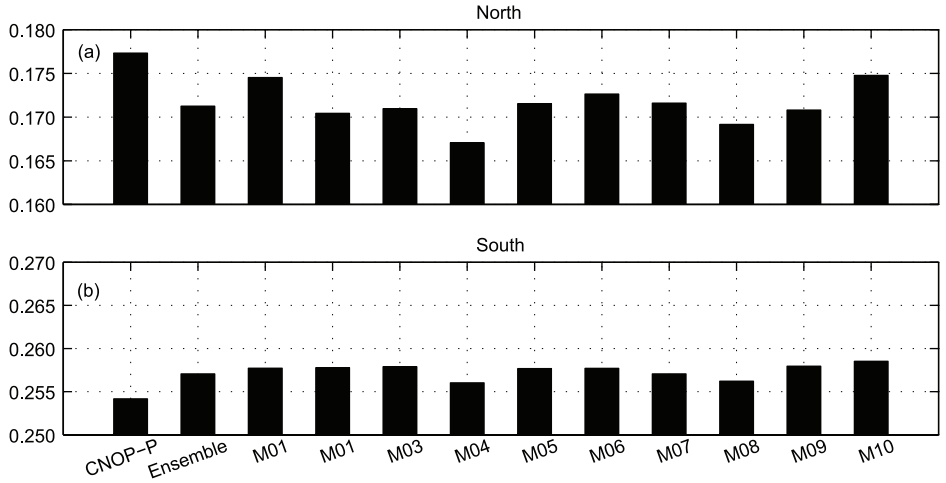

Figure 6 The annual SSLW in the final year (the year 2000) of the study period averaged in the north (a) and south (b) of 36°N under the CNOP-P-type and GCM-based future possible temperature change scenarios (m^3 m^{-3}).

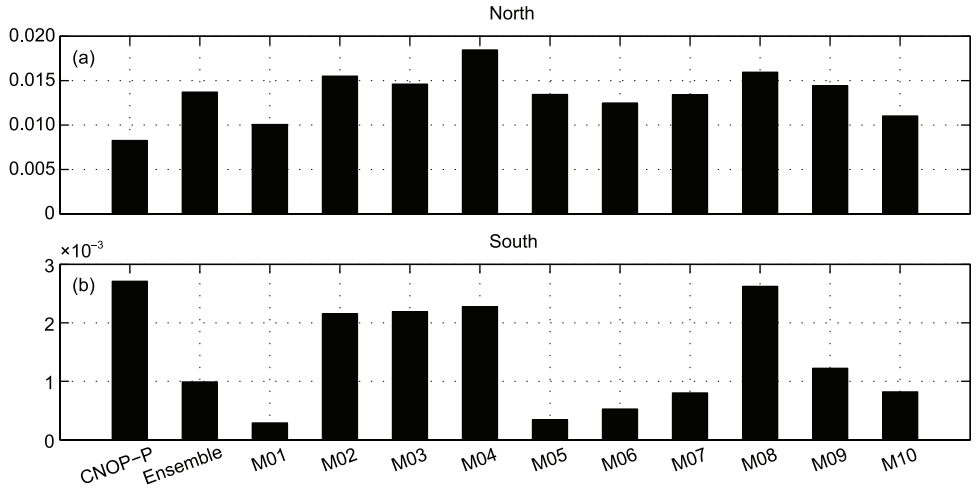

Figure 7 The annual surface soil ice in the final year (the year 2000) of the study period averaged in the north (a) and south (b) of 36°N under the CNOP-P-type and GCM-based future possible temperature change scenarios (m^3 m^{-3}).

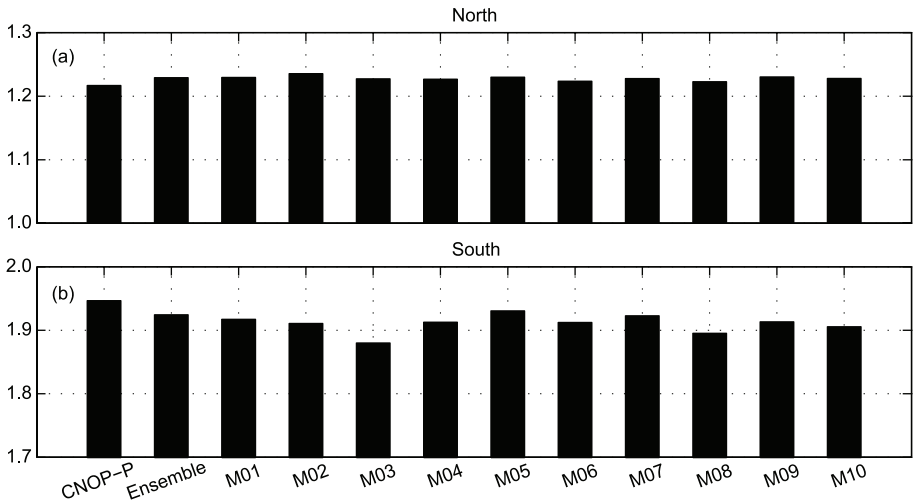

Figure 8 The annual evapotranspiration (ET) in the final year (the year 2000) of the study period averaged in the north (a) and south (b) of 36°N under the CNOP-P-type and GCM-based future possible temperature change scenarios (mm day^{-1}).

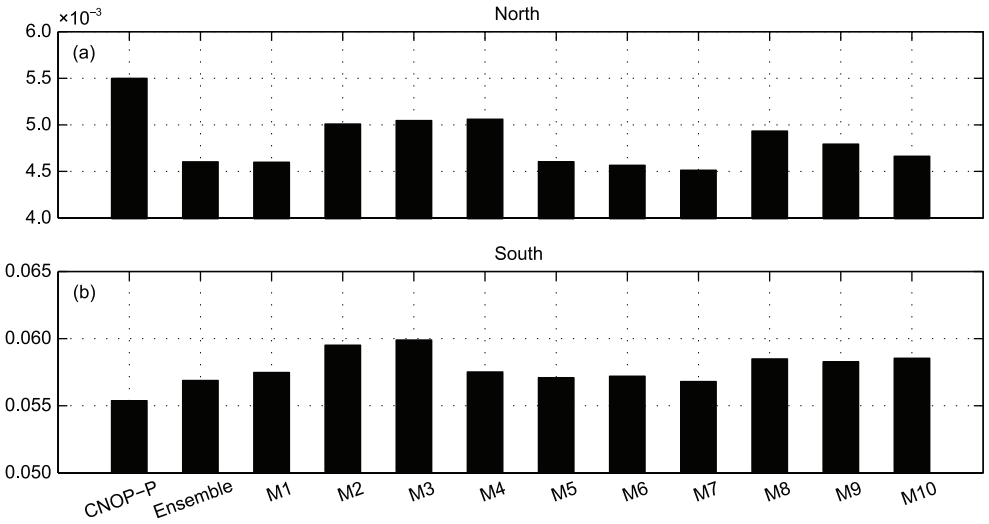

Figure 9 The annual surface runoff (Rsur) in the final year (the year 2000) of the study period averaged in the north (a) and south (b) of 36°N under the CNOP-P-type and GCM-based future possible temperature change scenarios (mm day^{-1}).

the monthly reference precipitation data in our study. In each month, the percent change of the monthly reference precipitation, caused by the superposed monthly perturbation, was added to the precipitation data of each model step in 30-minute intervals in the month to drive the CoLM model. However, the precipitation perturbation generated by the iterative process of the DE algorithm might be negative and even make the new precipitation data negative, which is not reasonable. In addition, the monthly reference precipitation data in some months may be zero. We have not determined a proper approach to allocate the non-zero precipitation perturbation into each model step of these months with zero monthly reference precipitation. Furthermore, the precipitation of each model step at 30-minute intervals could be added to the precipitation perturbation. However, it will be costly to obtain the CNOP-P. Thus, in this study, only the temperature change is considered. In future studies, the responses of SSLW to the regional and seasonal precipitation changes are worth exploring and should be higher than those to the regional and seasonal temperature changes if the proper condition is employed, or the computer is powerful enough.

4.2 The variations of SSLW

Currently, few studies have focused on the impacts of climate change on soil moisture, especially in China. Dan et al. (2012) applied the hypothesized climate change scenarios associated with temperature or precipitation and the VIC model to evaluate the possible hydrological changes in the 3H region of China (here, the 3H region is smaller than our study region). Under the conditions of increased temperature and no changes in precipitation, the spatial pattern that soil moisture increased in the north and decreased in the south with the boundary at approximately 35°N was shown in their study, which is similar to our results. In addition, Yang et al. (2003) also discussed the response of the soil moisture to the increasing temperature with the WAVES (WAter Vegetation Energy and Solute modeling) model on Taihang Mountain, China. The soil moisture would decrease from 0 to 8 mm. Their studies are consistent with our studies. Komuscu et al. (1998) also found that the soil moisture varied from 0% to –7% for some sites. By using the outputs of 11 CMIP5 models under the RCP4.5 scenario, Dai (2012) directly analyzed the percentage changes of SSLW from 1980–1999 to 2080–2099 and revealed that SSLW decreased in southeast China, where the reports of IPCC 5 (Collins et al., 2013) also displayed similar SSLW changes in the CMIP5 ensemble at the end of the 21st century under the RCP4.5 and RCP8.5 scenario. Specifically, the potential future SSLW changes in the '3H' region are shown in Figure 11 by directly analyzing the SSLW data from 7 CMIP5 GCMs (shown in bold font in Table 1), which have been bilinearly interpolated to the resolution of 1°×1°. For the 7 GCMs, the soil moisture data are obtained from the CMIP5 data, and these are high-resolution models. Our study region is propitious to the model with high resolution. If the model resolution is low, there are few grids. The interpolated data with little data is insufficient. Thus, the 7 GCMs are chosen. The multi-model ensemble mean indicates an increase of SSLW north of approximately 35°N and a decrease in the remaining region even though there is a large difference among the SSLW changes projected by different GCMs. However, for the lack of assessments of these global-scale models in their ability to simulate soil moisture (Flato et al., 2013), these results should be interpreted with caution.

In this paper, the '3H' region in China is chosen to investigate the influence of temperature change on SSLW. There are many important regions worth exploring the SSLW changes, such as Northeastern China, Southern China, and the arid and

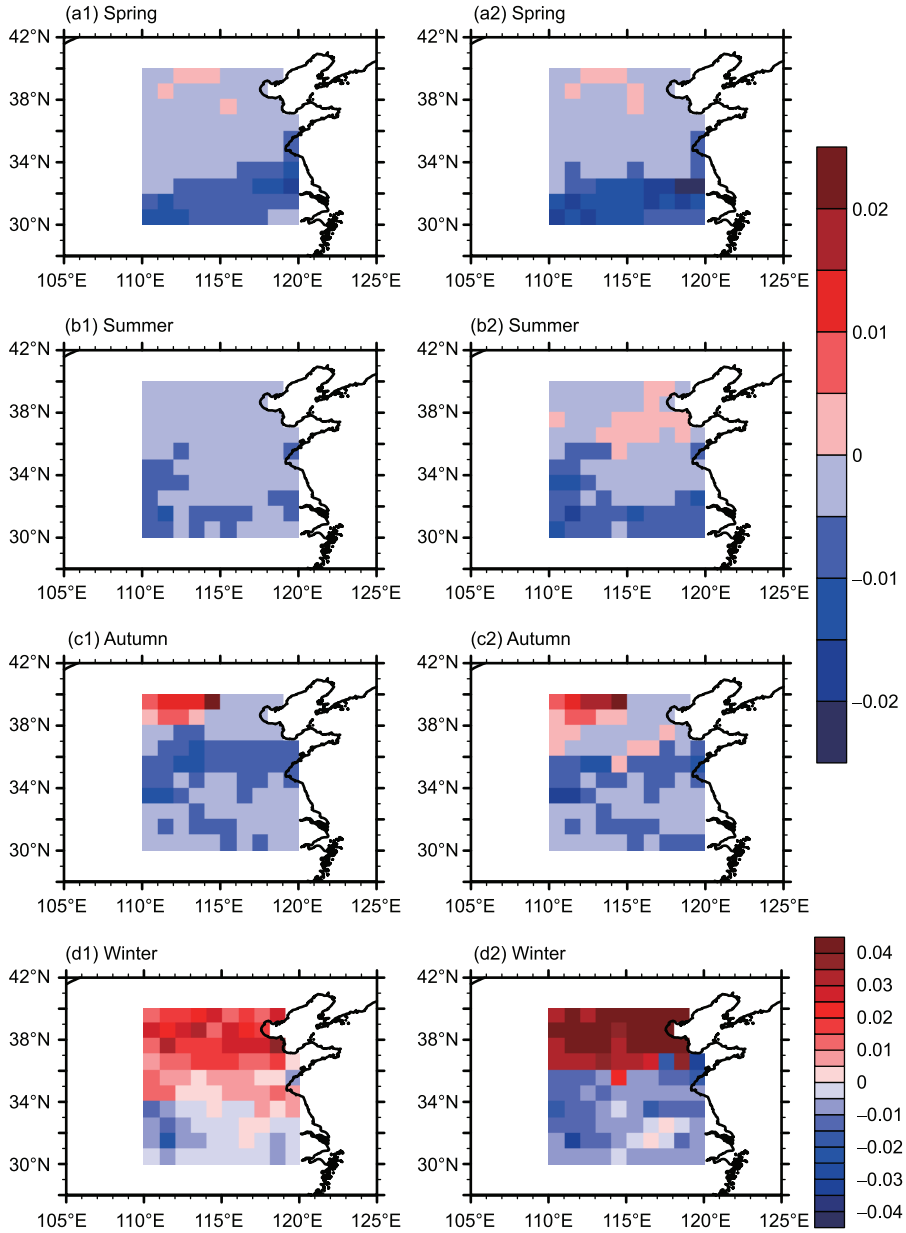

Figure 10 The SSLW changes in spring ((a1), (a2)), summer ((b1), (b2)), autumn ((c1), (c2)) and winter ((d1), (d2)) due to the ensemble temperature change series and the CNOP-P-type temperature change scenario (m^3 m^{-3}).

semi-arid region of China. Because the computational cost is expensive to obtain the CNOP-P-type temperature change scenario, only the '3H' region is chosen. In the future, other regions could be chosen to discuss the impact of climate change on SSLW.

5. Summary

To explore the maximal SSLW changes due to the seasonal and regional temperature change in the '3H' region of China, the CNOP-P approach and the projected outputs from 10 GCMs from CMIP5 are combined in this study. Based on the projected uncertainty range of the seasonal temperature change for 10 GCMs from CMIP5 under a high-emission scenario (the RCP8.5 scenario), the maximum possible responses of SSLW to future temperature change are determined by using the CoLM model. In addition, the seasonal temperature change scenario, which is acquired by applying the CNOP-P method and leads to the maximum SSLW change magnitudes, is denoted as the CNOP-P-type temperature change scenario. For comparison, the monthly temperature change series derived from each GCM, along with their ensemble average, are also considered to be a future type of potential temperature change scenario (11 scenarios in total) and used to explore the possible impacts of temperature change on SSLW.

Table 2 The regional averaged SSLW ($m^3\ m^{-3}$) in all seasons of the final year in the study period due to each temperature change scenario[a)]

Scenario	Region	Spring	Summer	Autumn	Winter
CNOP-P	'N'	0.1547	0.2130	0.2110	0.1300
	'S'	0.1988	0.2804	0.3026	0.2342
Ensemble	'N'	0.1550	0.2114	0.2082	0.1097
	'S'	0.2009	0.2812	0.3031	0.2426
M01	'N'	0.1539	0.2114	0.2077	0.1246
	'S'	0.2007	0.2815	0.3032	0.2449
M02	'N'	0.1556	0.2119	0.2091	0.1043
	'S'	0.2025	0.2830	0.3043	0.2408
M03	'N'	0.1551	0.2118	0.2094	0.1069
	'S'	0.2028	0.2824	0.3054	0.2404
M04	'N'	0.1551	0.2119	0.2091	0.0910
	'S'	0.2013	0.2815	0.3036	0.2373
M05	'N'	0.1549	0.2118	0.2082	0.1105
	'S'	0.2007	0.2815	0.3031	0.2448
M06	'N'	0.1549	0.2115	0.2086	0.1146
	'S'	0.2004	0.2814	0.3033	0.2452
M07	'N'	0.1552	0.2116	0.2090	0.1096
	'S'	0.2008	0.2812	0.3030	0.2426
M08	'N'	0.1548	0.2115	0.2091	0.1006
	'S'	0.2014	0.2819	0.3039	0.2371
M09	'N'	0.1549	0.2115	0.2085	0.1075
	'S'	0.2033	0.2820	0.3035	0.2425
M10	'N'	0.1552	0.2123	0.2086	0.1222
	'S'	0.2009	0.2828	0.3045	0.2454

a) 'N': North of 36°N; 'S': South of 36°N

Table 3 The regional averaged surface soil ice ($m^3\ m^{-3}$) in all seasons of the final year in the study period due to each temperature change scenario[a)]

Scenario	Region	Spring	Summer	Autumn	Winter
CNOP-P	'N'	0.0002	0.0000	0.0005	0.0324
	'S'	0.0000	0.0000	0.0000	0.0109
Ensemble	'N'	0.0004	0.0000	0.0008	0.0538
	'S'	0.0000	0.0000	0.0000	0.0040
M01	'N'	0.0010	0.0000	0.0012	0.0380
	'S'	0.0000	0.0000	0.0000	0.0012
M02	'N'	0.0003	0.0000	0.0009	0.0611
	'S'	0.0000	0.0000	0.0000	0.0086
M03	'N'	0.0004	0.0000	0.0009	0.0573
	'S'	0.0000	0.0000	0.0000	0.0088
M04	'N'	0.0005	0.0000	0.0006	0.0733
	'S'	0.0000	0.0000	0.0000	0.0091
M05	'N'	0.0006	0.0000	0.0007	0.0527
	'S'	0.0000	0.0000	0.0000	0.0014
M06	'N'	0.0003	0.0000	0.0009	0.0490
	'S'	0.0000	0.0000	0.0000	0.0021
M07	'N'	0.0003	0.0000	0.0003	0.0534
	'S'	0.0000	0.0000	0.0000	0.0033
M08	'N'	0.0003	0.0000	0.0007	0.0628
	'S'	0.0000	0.0000	0.0000	0.0105
M09	'N'	0.0010	0.0000	0.0008	0.0562
	'S'	0.0000	0.0000	0.0000	0.0049
M10	'N'	0.0004	0.0000	0.0023	0.0415
	'S'	0.0000	0.0000	0.0000	0.0033

a) 'N': North of 36°N; 'S': South of 36°N

Table 4 The regional averaged ET (mm day^{-1}) in all seasons of the final year in the study period due to each temperature change scenario[a)]

Scenario	Region	Spring	Summer	Autumn	Winter
CNOP-P	'N'	0.6949	2.2609	1.5721	0.3272
	'S'	1.9246	2.9779	1.8932	0.9809
Ensemble	'N'	0.7102	2.3251	1.5720	0.2956
	'S'	1.8978	2.9638	1.8700	0.9561
M01	'N'	0.6985	2.3053	1.5782	0.3226
	'S'	1.8379	2.9293	1.8706	1.0248
M02	'N'	0.7332	2.3330	1.5637	0.2981
	'S'	1.9384	2.9106	1.8537	0.9306
M03	'N'	0.7159	2.3289	1.5520	0.2987
	'S'	1.9105	2.9251	1.7706	0.9035
M04	'N'	0.7145	2.3217	1.5747	0.2826
	'S'	1.9251	2.9394	1.8701	0.9061
M05	'N'	0.7099	2.3074	1.5905	0.2986
	'S'	1.8752	2.9569	1.8674	1.0129
M06	'N'	0.7141	2.2963	1.5766	0.2937
	'S'	1.9186	2.9132	1.8773	0.9304
M07	'N'	0.7113	2.3146	1.5833	0.2874
	'S'	1.9200	2.9417	1.8849	0.9322
M08	'N'	0.7079	2.3204	1.5622	0.2878
	'S'	1.9156	2.9168	1.8597	0.8811
M09	'N'	0.7116	2.3283	1.5691	0.2983
	'S'	1.8804	2.9476	1.8595	0.9551
M10	'N'	0.7118	2.3101	1.5555	0.3201
	'S'	1.9100	2.9142	1.8073	0.9801

a) 'N': North of 36°N; 'S': South of 36°N

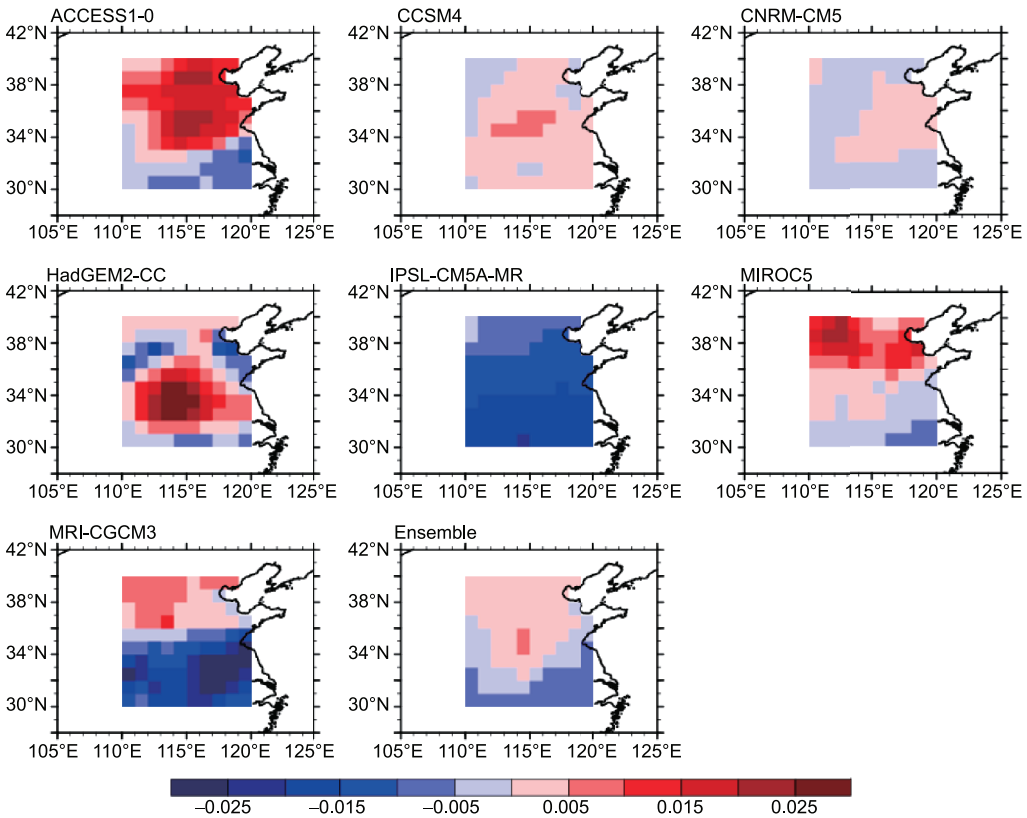

Figure 11 Future changes in SSLW (m^3 m^{-3}) simulated using 7 GCMs under the RCP8.5 scenario from CMIP5: averaged variations of the SSLW mean state every 10 years from 2011 to 2100 compared to the study period 1991–2000.

Generally, the proposed 12 temperature change scenarios, all of which characterize the seasonal and regional heterogeneity of future temperature change, lead to nearly the same SSLW sign changes in the entire '3H' region. Take 36°N as a boundary. In the northern region, the temperature perturbations make SSLW increase by contributing to the soil ice melting. In the southern region, temperature change makes SSLW decrease primarily through enhancing *ET*. However, the CNOP-P-type temperature change scenario causes the maximal SSLW change magnitudes, which could indicate the maximal possible uncertainty extent of SSLW changes induced by future possible temperature change alone. Specifically, the CNOP-P-type temperature scenario makes the regional SSLW increase by 0.0099 $m^3\ m^{-3}$ in the north and decrease by 0.0070 $m^3\ m^{-3}$ in the south.

In addition, the SSLW variations in each season caused by the 12 potential temperature change scenarios are also examined. It is found that SSLW decreases in all seasons expect winter in the north of 36°N. The SSLW change in winter dominates the annual SSLW variation and results in the increase in annual SSLW in this region. Over the remaining region, SSLW decreases in all seasons due to the seasonal temperature change, especially in spring. Conversely, the responses of the SSLW to other meteorological factors are also sensitive, such as precipitation. However, the impact of temperature change on the SSLW is just explored in the current study. Although the reason to exclude the impact of precipitation is discussed in the above study, the response of SSLW to other meteorological factors, such as precipitation, should be demonstrated, and the limitation of this study will be overcome in future studies.

Acknowledgements *This work was supported by the National Natural Science Foundation of China (Grant Nos. 91437111 & 41375111 & 41675104 & 41230420).*

References

Aich V, Liersch S, Vetter T, Huang S, Tecklenburg J, Hoffmann P, Koch H, Fournet S, Krysanova V, Müller E N, Hattermann F F. 2014. Comparing impacts of climate change on streamflow in four large African river basins. Hydrol Earth Syst Sci, 18: 1305–1321

Bastola S, Murphy C, Sweeney J. 2011. The role of hydrological modelling uncertainties in climate change impact assessments of Irish river catchments. Adv Water Resour, 34: 562–576

Bonan G B, Stillwell-Soller L M. 1998. Soil water and the persistence of floods and droughts in the Mississippi River Basin. Water Resour Res, 34: 2693–2701

Chen H, Xu C Y, Guo S. 2012. Comparison and evaluation of multiple GCMs, statistical downscaling and hydrological models in the study of climate change impacts on runoff. J Hydrol, 434-435: 36–45

Chen J, Brissette F P, Chaumont D, Braun M. 2013. Performance and uncertainty evaluation of empirical downscaling methods in quantifying the climate change impacts on hydrology over two North American river basins. J Hydrol, 479: 200–214

Chen L, Duan W S, Xu H. 2015. A SVD-based ensemble projection algorithm for calculating the conditional nonlinear optimal perturbation. Sci China Earth Sci, 58: 385–394

Chen L, Frauenfeld O W. 2014a. A comprehensive evaluation of precipitation simulations over China based on CMIP5 multimodel ensemble projections. J Geophys Res-Atmos, 119: 5767–5786

Chen L, Frauenfeld O W. 2014b. Surface air temperature changes over the Twentieth and Twenty-First Centuries in China simulated by 20 CMIP5 models. J Clim, 27: 3920–3937

Collins M, Knutti R, Arblaster J, Dufresne J L, Fichefet T, Friedlingstein P, Gao X, Gutowski W J, Johns T, Krinner G, Shongwe M, Tebaldi C, Weaver A J, Wehner M. 2013. Long-term Climate Change: Projections, Commitments and Irreversibility. In: Stocker T F, Qin D, Plattner G K, Tignor M, Allen S K, Boschung J, Nauels A, Xia Y, Bex V, Midgley P M, eds. Climate Change 2013: The Physical Science Basis. Contribution of Working Group I to the Fifth Assessment Report of the Intergovernmental Panel on Climate Change. Cambridge: Cambridge University Press. 1079–1080

Conil S, Douville H, Tyteca S. 2006. The relative influence of soil moisture and SST in climate predictability explored within ensembles of AMIP type experiments. Clim Dyn, 28: 125–145

Dai A. 2012. Increasing drought under global warming in observations and models. Nat Clim Change, 3: 52–58

Dai Y, Zeng X, Dickinson R E, Baker I, Bonan G B, Bosilovich M G, Denning A S, Dirmeyer P A, Houser P R, Niu G, Oleson K W, Schlosser C A, Yang Z L. 2003. The common land model. Bull Amer Meteorol Soc, 84: 1013–1023

Dan L, Ji J, Xie Z, Chen F, Wen G, Richey J E. 2012. Hydrological projections of climate change scenarios over the 3H region of China: A VIC model assessment. J Geophys Res, 117: D11102

Ding Y, Ren G, Shi G, Gong P, Zheng X, Zhai P, Zhang D, Zhao Z, Wang S, Wang H, Luo Y, Chen D, Gao X, Dai X. 2006. National Assessment Report of Climate Change (I): Climate change in China and its future trend (in Chinese). Adv Climate Change Res, V02: 3–8

Dobler C, Hagemann S, Wilby R L, Stötter J. 2012. Quantifying different sources of uncertainty in hydrological projections in an Alpine watershed. Hydrol Earth Syst Sci, 16: 4343–4360

Duan W, Zhang R. 2010. Is model parameter error related to a significant spring predictability barrier for El Niño events? Results from a theoretical model. Adv Atmos Sci, 27: 1003–1013

Flato G, Marotzke J, Abiodun B, Braconnot P, Chou S C, Collins W, Cox P, Driouech F, Emori S, Eyring V, Forest C, Gleckler P, Guilyardi E, Jakob C, Kattsov V, Reason C, Rummukainen M. 2013. Evaluation of Climate Models. In: Stocker T F, Qin D, Plattner G K, Tignor M, Allen S K, Boschung J, Nauels A, Xia Y, Bex V, Midgley P M, eds. Climate Change 2013: The Physical Science Basis, Contribution of Working Group I to the Fifth Assessment Report of the Intergovernmental Panel on Climate Change. Cambridge: Cambridge University Press. 790–791

Hirschi M, Seneviratne S I, Alexandrov V, Boberg F, Boroneant C, Christensen O B, Formayer H, Orlowsky B, Stepanek P. 2011. Observational evidence for soil-moisture impact on hot extremes in southeastern Europe. Nat Geosci, 4: 17–21

Komuscu A U, Erkan A, Oz S. 1998. Possible impacts of climate change on soil moisture availability in the southeast anatolia development project region (GAP): An analysis from an agricultural drought perspective. Clim Change, 40: 519–545

Koster R D, Suarez M J, Liu P, Jambor U, Berg A, Kistler M, Reichle R, Rodell M, Famiglietti J. 2004. Realistic initialization of land surface states: Impacts on subseasonal forecast skill. J Hydrometeorol, 5: 1049–1063

Li M, Ma Z. 2010. Comparisons of simulations of soil moisture variations in the Yellow River basin driven by various atmospheric forcing data sets. Adv Atmos Sci, 27: 1289–1302

Liu L, Zhang R, Zuo Z. 2014. Intercomparison of spring soil moisture among

multiple reanalysis data sets over eastern China. J Geophys Res-Atmos, 119: 54–64
Liu S, Lin Z. 2005. Validation of common land model using field experiment data over typical land cover types in East Asia (in Chinese). Clim Environ Res, 10: 684–699
Lorenz R, Jaeger E B, Seneviratne S I. 2010. Persistence of heat waves and its link to soil moisture memory. Geophys Res Lett, 37: L09703
Ma Z G, Fu C B. 2005. Decadal variations of arid and semi-arid boundary in China (in Chinese). Chin J Geophys, 48: 519–525
Mehrotra R. 1999. Sensitivity of runoff, soil moisture and reservoir design to climate change in central Indian River Basins. Clim Change, 42: 725–757
Mu M, Duan W, Wang Q, Zhang R. 2010. An extension of conditional nonlinear optimal perturbation approach and its applications. Nonlin Processes Geophys, 17: 211–220
Peng F, Mu M, Sun G D. 2017. Responses of soil moisture to climate change based on projections by the end of the 21st century under the high emission scenario in the 'Huang-Huai-Hai Plain' region of China. J Hydro-environment Res, 14: 105–118
Ren G, Ding Y, Zhao Z, Zheng J, Wu T, Tang G, Xu Y. 2012. Recent progress in studies of climate change in China. Adv Atmos Sci, 29: 958–977
Sheffield J, Goteti G, Wood E F. 2006. Development of a 50-year high-resolution global dataset of meteorological forcings for land surface modeling. J Clim, 19: 3088–3111
Song Y, Guo W, Zhang Y, Chen Y. 2009. Performances of CoLM and NCAR_CLM3.0 in simulating land-atmosphere interactions over typical forest ecosystems in China Part I. Preliminary analysis of the simulations based on different models (in Chinese). Clim Environ Res, 14: 229–242
Sperna Weiland F C, van Beek L P H, Weerts A H, Bierkens M F P. 2012. Extracting information from an ensemble of GCMs to reliably assess future global runoff change. J Hydrol, 412–413: 66–75
Sun G D, Mu M. 2011. Nonlinearly combined impacts of initial perturbation from human activities and parameter perturbation from climate change on the grassland ecosystem. Nonlin Processes Geophys, 18: 883–893
Sun G D, Mu M. 2012. Responses of soil carbon variation to climate variability in China using the LPJ model. Theor Appl Climatol, 110: 143–153
Sun G D, Mu M. 2013. Understanding variations and seasonal characteristics of net primary production under two types of climate change scenarios in China using the LPJ model. Clim Change, 120: 755–769
Sun G D, Mu M. 2014. The analyses of the net primary production due to regional and seasonal temperature differences in eastern China using the LPJ model. Ecol Model, 289: 66–76
Sun G D, Mu M. 2017a. A new approach to identify the sensitivity and importance of physical parameters combination within numerical models using the Lund-Potsdam-Jena (LPJ) model as an example. Theor Appl Climatol, 128: 587–601
Sun G D, Mu M. 2017b. Projections of soil carbon using the combination of the CNOP-P method and GCMs from CMIP5 under RCP4.5 in north-south transect of eastern China. Plant Soil, 413: 243–260
Taylor K E, Stouffer R J, Meehl G A. 2012. An overview of CMIP5 and the experiment design. Bull Amer Meteorol Soc, 93: 485–498
Tao F, Yokozawa M, Hayashi Y, Lin E. 2003. Future climate change, the agricultural water cycle, and agricultural production in China. Agriculture Ecosystems Environ, 95: 203–215
Wang A, Lettenmaier D P, Sheffield J. 2011. Soil moisture drought in China, 1950–2006. J Clim, 24: 3257–3271
Wang G Q, Zhang J Y, Jin J L, Pagano T C, Calow R, Bao Z X, Liu C S, Liu Y L, Yan X L. 2012. Assessing water resources in China using PRECIS projections and a VIC model. Hydrol Earth Syst Sci, 16: 231–240
Wang Q, Mu M, Dijkstra H A. 2012. Application of the conditional nonlinear optimal perturbation method to the predictability study of the Kuroshio large meander. Adv Atmos Sci, 29: 118–134
Wang J D, Guo W D, Li H Q. 2013. Application of extended Fourier amplitude sensitivity test (EFAST) method in land surface parameter sensitivity analysis. Acta Phys Sin, 62: 050202
Wu L Y, Zhang J Y. 2013. Role of land-atmosphere coupling in summer droughts and floods over eastern China for the 1998 and 1999 cases. Chin Sci Bull, 58: 3978–3985
Xin Y, Bian L, Zhang X. 2006. The application of CoLM to arid region of northwest China and Qinghai-Xizang Plateau. Plateau Meteorol, 25: 567–574
Yang K, Ye B, Zhou D, Wu B, Foken T, Qin J, Zhou Z. 2011. Response of hydrological cycle to recent climate changes in the Tibetan Plateau. Clim Change, 109: 517–534
Yang Y, Watanabe M, Wang Z, Sakura Y, Tang C. 2003. Prediction of changes in soil moisture associated with climatic changes and their implications for vegetation changes: Waves model simulation on Taihang Mountain, China. Clim Change, 57: 163–183
Zeng X, Shaikh M, Dai Y, Dickinson R E, Myneni R. 2002. Coupling of the common land Model to the NCAR community climate model. J Clim, 15: 1832–1854
Zhang R, Zuo Z. 2011. Impact of spring soil moisture on surface energy balance and summer monsoon circulation over east asia and precipitation in East China. J Clim, 24: 3309–3322
Zhang R, Wu B, Han J, Zuo Z. 2013. Effects on summer monsoon and rainfall change over China due to Eurasian snow cover and ocean thermal conditions. In: Singh B R, ed. Climate Change-Realities, Impacts over Ice Cap, Sea Level and Risks, InTech. Rijeka. 227–250
Zhang R. 2015. Changes in East Asian summer monsoon and summer rainfall over eastern China during recent decades. Chin Sci Bull, 60: 1222–1224
Zuo Z Y, Zhang R H. 2007. The spring soil moisture and the summer rainfall in eastern China. Chin Sci Bull, 52: 3310–3312